Chinese Physics Letters

中国物理学会 Chinese Physical Society

PAPER

Effects of Localized Interface Phonons on Heat Conductivity in Ingredient Heterogeneous Solids

To cite this article: Mei Wu *et al* 2023 *Chinese Phys. Lett.* **40** 036801

View the article online for updates and enhancements.

You may also like

- Ultimate optimization of interface thermal resistance by utilizing interfacial nonlinear interaction
Lei Xu, Tingting Wang, Kaiyang Zhang et al.
- Investigation of ambient temperature and thermal contact resistance induced self-heating effects in nanosheet FET
Sunil Rathore, Rajeewa Kumar Jaisawal, Preeti Suryavanshi et al.
- Bidirectional and Unidirectional Negative Differential Thermal Resistance Effect in a Modified Lorentz Gas Model
Yu Yang, , XiuLing Li et al.

This content was downloaded from IP address 162.105.59.157 on 06/09/2023 at 10:17

Effects of Localized Interface Phonons on Heat Conductivity in Ingredient Heterogeneous Solids

Mei Wu(武媚)[1,2†], Ruochen Shi(时若晨)[1,2†], Ruishi Qi(亓瑞时)[1,2,3†], Yuehui Li(李跃辉)[1,2], Tao Feng(冯涛)[4,5], Bingyao Liu(刘秉尧)[2], Jingyuan Yan(严靖园)[2], Xiaomei Li(李晓梅)[1,2], Zhetong Liu(刘哲彤)[2], Tao Wang(王涛)[2], Tongbo Wei(魏同波)[4,5], Zhiqiang Liu(刘志强)[4,5], Jinlong Du(杜进隆)[2], Ji Chen(陈基)[6,7], and Peng Gao(高鹏)[1,2,7,8,9*]

[1]*International Center for Quantum Materials, Peking University, Beijing 100871, China*
[2]*Electron Microscopy Laboratory, School of Physics, Peking University, Beijing 100871, China*
[3]*Department of Physics, University of California at Berkeley, Berkeley 94720, USA*
[4]*Research and Development Center for Semiconductor Lighting Technology, Institute of Semiconductors, Chinese Academy of Sciences, Beijing 100083, China*
[5]*Center of Materials Science and Optoelectronics Engineering, University of Chinese Academy of Sciences, Beijing 100049, China*
[6]*State Key Laboratory for Mesoscopic Physics, School of Physics, Peking University, Beijing 100871, China*
[7]*Collaborative Innovation Center of Quantum Matter, Beijing 100871, China*
[8]*Interdisciplinary Institute of Light-Element Quantum Materials and Research Center for Light-Element Advanced Materials, Peking University, Beijing 100871, China*
[9]*Hefei National Laboratory, Hefei 230088, China*

(Received 8 January 2023; accepted manuscript online 15 February 2023)

Phonons are the primary heat carriers in non-metallic solids. In compositionally heterogeneous materials, the thermal properties are believed to be mainly governed by the disrupted phonon transport due to mass disorder and strain fluctuations, while the effects of compositional fluctuation induced local phonon states are usually ignored. Here, by scanning transmission electron microscopy electron energy loss spectroscopy and sophisticated calculations, we identify the vibrational properties of ingredient-dependent interface phonon modes in $Al_xGa_{1-x}N$ and quantify their various contributions to the local interface thermal conductance. We demonstrate that atomic-scale compositional fluctuation has significant influence on the vibrational thermodynamic properties, highly affecting the mode ratio and vibrational amplitude of interface phonon modes and subsequently redistributing their modal contribution to the interface thermal conductance. Our work provides fundamental insights into understanding of local phonon-boundary interactions in nanoscale inhomogeneities, which reveal new opportunities for optimization of thermal properties via engineering ingredient distribution.

DOI: 10.1088/0256-307X/40/3/036801

Thermal conductivity describes heat dissipation capability inside materials, being a key factor in thermoelectric energy conversion[1,2] and thermal management of electronic devices.[3–6] For heterogeneous materials, fluctuations in local concentration typically hold the key to determine thermal properties[1,7,8] even and particularly at the nanoscale. For example, many recent great advances in designing high-performance thermoelectric materials are linked to modulation of nanoscale ingredient inhomogeneity.[7,9] These nanoscale controls such as doping, alloying and nanoprecipitation will disrupt the phonon transport and subsequently decrease the thermal conductivity.[10,11] Previous conventional consideration about these nanoscale phenomena mainly focuses on the mass disorder and strain fluctuations, which assumes the random mixture of atoms with different masses and volumes in a lattice[9,12] and has been well studied.[13,14] However, the influence of boundaries/interfaces induced by ingredient variation in inhomogeneous solids is usually oversimplified,[15–17] much less than a clear cognition of the relation between the ingredient changes and interface thermal conductance (ITC) changes. In fact, the previous theoretical work observed that the superlattice thermal conductivity was lower than that of the alloy with the same mass ratios,[18,19] indicating the important contributions of the ITC and thus calling for unraveling the unique thermal properties of interfaces.

The proper knowledge of the thermal transport mechanisms occurring at the compositional interface requires considering the local phonon modes. Previous extensively accepted descriptions about the ITC, such as the acoustic mismatch model and the diffuse mismatch model for the phonon transport, mainly consider the mismatch of the phonon density of states (DOS) between constituent bulk materials.[20] In fact, thermal properties of materials are rooted in their microstructures. Due to different bonds at the interface, unique eigen solutions are required to describe the equations of atomic vibrational motion compared to the bulks.[21] Indeed, there are more and more theoretical works concerning the important role of such

†These authors contributed equally to this work.
*Corresponding author. Email: pgao@pku.edu.cn
© 2023 Chinese Physical Society and IOP Publishing Ltd

localized modes (eigenmodes with large displacements for interfacial atoms) on the ITC.[22–24] Unfortunately, experimentally the heat dissipation at an interface still cannot be dealt with confidently, mainly owing to the lack of ability in probing local phonon DOS, dispersion relation and scattering mechanism at the interface, arising from the inadequate spatial resolutions in conventional experimental measurements.[25–27] How to bridge the theoretical calculation with experimental results is also essential for well understanding the nature of phonon-interface scattering.

In this Letter, we use the advanced vibrational electron energy loss spectroscopy (EELS) technique in scanning transmission electron microscopy (STEM)[28–35] combined with sophisticated density functional perturbation theory (DFPT) calculations and molecular dynamics (MD) calculations, trying to provide a direct physical picture of the correlation among the ingredient change, lattice dynamics and thermal properties at the atomic scale. We choose the $Al_xGa_{1-x}N$-based interface system, which is extensively used in highly integrated microelectronic products and optical devices.[36,37] To reveal the fundamental mechanism of phonon-interface scattering, we first study the GaN/AlN interface, confirming the existence of localized interface phonon modes from the atomically resolved phonon DOS measurements and mapping the phonon dispersion across the interface with nanometer atomic resolution. These interface phonon modes are highly localized within ~ 1.5 nm and make significant contribution to the ITC. For the $Al_xGa_{1-x}N$/AlN system, it shows similar interface phonon characteristics with GaN/AlN interface. However, these interface phonon modes are sensitive to compositional fluctuation. We demonstrate that as the Al fraction increases, the number of states and vibrational amplitude for the localized modes are reduced, subsequently showing lower degree of interaction with other modes and contributing less ITC. Our work provides insights of the fundamental phonon transport physics with the nanoscale and atomic-scale compositional fluctuations in heterogeneous materials. The engineering of vibrational thermodynamics over compositional intertwining can also help to optimize efficient thermal managements in material science.

Figure 1 gives a schematic illustration of the distinctive nanostructured geometry in heterogeneous media. Ideally, the different ingredients are fully mixed [Fig. 1(b)], introducing mass contrast and strain field fluctuations. In practice, the local concentrations are always varied in stable compounds. For example, nanophase segregations and nanoprecipitations commonly exist in thermoelectric materials, ubiquitously resulting in the emergence of interfaces. Generally, we can separate the inhomogeneity with different kinds of boundaries, some of which shows fully sharp ingredient-separated interface structure [Fig. 1(c)] and others shows element interdiffusion [Fig. 1(d)]. As observed by previous theoretical work, the superlattice thermal conductivity was lower than that of the alloy with the same mass ratios,[18,19] indicating that the compositional interface plays an important role in the thermal conductivity.

Hence, in order to give a thorough description of the phonon-interface scattering in nanoscale compositional fluctuations, we choose the $Al_xGa_{1-x}N$/AlN interface as a model system and first study the simplest but most essential GaN/AlN interface ($x = 0$). The atomically resolved high angle annular dark field (HAADF) image (Fig. S1 in the Supplementary Materials) and the integrated differential phase contrast (iDPC) image [Fig. 2(a)] show the atomically sharp and coherent interface. To obtain GaN/AlN interface vibration characteristics, the phonon spectra across the interface [Fig. 2(b)] are recorded in the off-axis setup with a large convergence angle, under which the acquired signal is close to local phonon DOS.[29,35,38] The experimental details are included in the Supplementary Materials (see Methods and Fig. S1). For better describing the phonon DOS variation, we extract the peak energy [Fig. 2(c)] by least-square fitting the measured spectrum to a sum of Lorentzian peaks. In the GaN side, the spectrum displays four major peaks at around 24 meV, 39 meV, 76 meV, and 85 meV, while in the AlN side, three peaks at around 38 meV, 65 meV, and 84 meV are distinguishable. When approaching the interface, the spectrum features change.

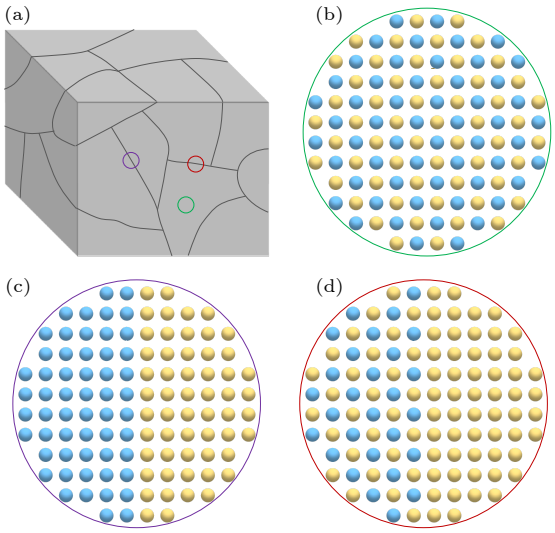

Fig. 1. Schematics of typical regions in heterogeneous media: (a) heterogeneous media with various boundaries/interfaces, (b) fully disordered heterogeneous media, (c) sharp compositional interface, (d) interface with chemical mixing in one side.

To give accurate and detailed phonon scattering mechanisms, we then performed DFPT calculations, which were performed within Quantum ESPRESSO[39] using the Perdew–Burke–Ernzerhof exchange-correlation functional[40] and ultrasoft pseudopotential.[41] The AlN/GaN interface model contains 8 layers of GaN atoms connected to 8 layers of AlN (32 atoms in one hexagonal unit cell with cell parameters $a = 3.173$ Å and $c = 41.048$ Å) (see Methods in Supplementary Materials for details). As shown in Fig. S2(a), bulk GaN and AlN have similar phonon dispersion profiles with large degree of overlap of phonon DOS, except that GaN features an obvious optical-optical gap due to a larger atomic mass difference between cation and anion.[42] The corresponding calculated projected DOS of each atom layer across the interface is illustrated in Fig. 2(d), which exhibits good agreement with the experimental data [Fig. 2(b)]. Specifically,

for GaN adjacent to the interface, the acoustic branch (at ∼24 meV) has slight blue shift. Moreover, as marked by the black arrows in Figs. 2(b)–2(d), the GaN layer adjacent to the interface vibrates at frequency above its maximum vibrational frequencies ($\omega_{\mathrm{max,GaN}}$) (from 85 meV to 89 meV approaching the interface), which is similar to the localized phonon modes at the Si/Ge interface with the frequency between the $\omega_{\mathrm{max,Si}}$ and $\omega_{\mathrm{max,Ge}}$.[43] In addition, the projected DOS at 80 meV is prominent in the GaN layer adjacent to the interface, accounting for the experimental observation on the blueshift of vibrational energy loss peak at 76 meV near the interface. On the AlN side, a slight red shift is observed for the peak at 65 meV approaching the interface. Such enhancement of phonon DOS overlap at the interface may mitigate the phonon mismatch between two materials and thus improve phonon transmission at the interface.

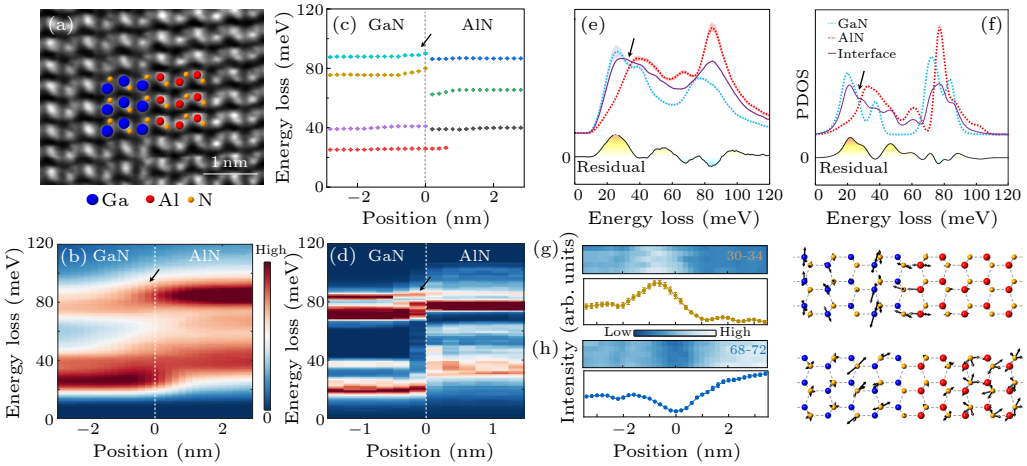

Fig. 2. Interface vibration at the GaN/AlN heterojunction: (a) iDPC image of the GaN/AlN interface viewed along [110] zone axis, illustrating the atomic structure of interface. Blue, red and yellow balls represent Ga, Al and N atoms, respectively. (b) Spectrum profile of measured off-axis phonon spectra across the interface. (c) Fitted peak positions of phonon spectra in (b) by least square fitting methods. (d) Calculated phonon DOS projected on atom layers across the interface. [(e), (f)] Extracted EEL spectra (e) and calculated projected DOS (f) from GaN (blue), AlN (red), and the interface (purple). The black curve indicates the interface component that cannot be expressed as a linear combination of two bulk spectra, showing similar trends. [(g), (h)] Spatial distribution mapping and corresponding intensity line profiles of localized (g) and isolated modes (h) extracted from (b). The energy integration windows are labeled in meV. The corresponding calculated phonon eigenvectors are shown in the right panel. Arrows illustrate the vibration amplitude of each atom.

For better understanding the local phonon behaviors at the interface, we extract the measured spectra [Fig. 2(e)] and calculated projected DOS [Fig. 2(f)] with the beam located in GaN (blue curve), in AlN (red curve), and at the interface (purple curve). We fit the interface spectrum with the linear combination of two bulk spectra to match the acquired spectra best. Then the residual part (black line) means the exceptional properties that only exist at the interface, where the experimental and calculated results show decent agreement. The corresponding experimental fitting residuals are also shown in Figs. S2(b) and S2(c). As can be seen, despite the large overlap of phonon DOS among GaN and AlN, the heterointerface between them certainly shows unique phonon modes. In order to further validate their presence, we extracted the energy-filtered EELS maps shown in Figs. 2(g) and 2(h). The intensity maps for 30–34 meV energy window [left panel in Fig. 2(g)] show an enhanced intensity at the interface within ∼1.5 nm in space. Such enhancement is also consistent with the positive residual and the higher intensity of interface spectrum at 30–34 meV energy window compared with bulk sides [marked by the black arrow in Figs. 2(e) and 2(f)], corresponding to the localized modes with enhanced vibration at the interface. What's more, we observe decreased intensity at the interface at 68–72 meV [left panel in Fig. 2(h)], corresponding to the negative residual and implying the isolated modes that both sides vibrate but the vibration amplitude is reduced at the interface. Their presence is also confirmed by the corresponding calculations of phonon eigenvectors [right panels in Figs. 2(g) and 2(h)]. Besides these two phonon modes, other classes of interface phonon modes (extended modes and partially extended modes, representing vibrations spread over the whole system and vibrations mainly exhibit at one side, respectively) maps are also recognized (Fig. S3).

Furthermore, we explore the dependence of vibrational energy on momentum across the interface with nanometer spatial resolution using the four-dimensional EELS (4D-EELS) technique.[34,44] Figure S4 shows typical phonon dispersion curves along $\Gamma KMK\Gamma$ viewing in $[1\bar{2}0]$ direction from experiments and corresponding simulations for GaN, in AlN, and the interface respectively. The reasonable agreement between the experiment and simulation further verifies the presence of complicated vibrational features at the interface, which are different from those in the bulks.

The following crucial question is the influence of compositional fluctuation and whether we can engineer the interface phonon behavior. Therefore, we explore the $Al_xGa_{1-x}N$/AlN system where one side ingredient is var-

ied. Figure 3(a) displays the atomic-resolution HAADF image, showing identical interface structure with the GaN/AlN system. The corresponding elemental distribution is also revealed by the line profiles of energy dispersive x-ray spectroscopy (EDS) [Fig. 3(b)]. The off-axis phonon spectra across the interface [Fig. 3(c)] show similar tendency with the GaN/AlN system but with unobtrusive fitting residual as shown in Fig. 3(d).

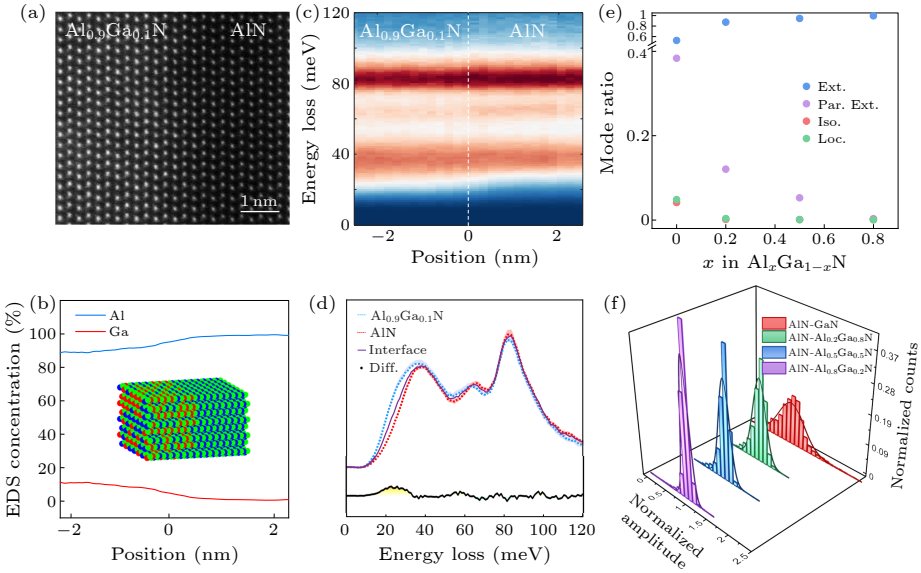

Fig. 3. Interface phonon mapping for the $Al_xGa_{1-x}N$/AlN interface: [(a), (b)] HAADF image (a) and corresponding EDS mapping (b) of the $Al_{0.9}Ga_{0.1}N$/AlN interface. (c) Line profile of measured off-axis phonon spectra across the interface. (d) Extracted EEL spectra from $Al_{0.9}Ga_{0.1}$ N (blue), AlN (red), and the interface (purple). The black curve indicates the interface component that cannot be expressed as a linear combination of two bulk spectra. (e) Calculated number of states for the four different classes of interface phonon modes with the change of Al fraction in $Al_xGa_{1-x}N$. Ext.: extended modes. Par. Ext.: partial extended modes. Iso: isolated modes. Loc: localized modes. (f) Calculated distribution of normalized interface vibration amplitude with the change of Al fraction in $Al_xGa_{1-x}N$.

To systematically and qualitatively interpret the vibrational spectra of $Al_xGa_{1-x}N$/AlN system, we built supercell with 7×8 in-plane expansion based on the above DFT-optimized GaN/AlN atomic configuration and randomly replaced Ga atoms by Al atoms with ratio x in each atomic plane. The dynamical matrix was built under mass approximation, i.e., the interatomic force constants are assumed to be invariant to composition ratio x. The corresponding typical model are illustrated in Fig. 3(b). The phonon modes were classified into one of extended mode (Ext.), partially extended mode (Par Ext.), isolated mode (Iso.) or localized mode (Loc.), by their amplitude distribution over space.[45] The criteria for classification in AlN/B ($B = Al_xGa_{1-x}N$) are as follows:

$$P_{i,\mathrm{tot}} = \sum_{j\in \text{entire system}} |e_{ij}|,$$

$$P_{i,\mathrm{int}} = \sum_{j\in \text{interface region}} |e_{ij}|,$$

$$P_{i,\mathrm{AlN}} = \sum_{j\in \mathrm{AlN}} |e_{ij}|,$$

$$P_{i,B} = \sum_{j\in B} |e_{ij}|,$$

where e_{ij} represents the vibration amplitude of atom j and eigen mode i. The interface region contains the atoms within three atomic layers (~ 0.8 nm) from the interface plane. The four types of interface modes are defined as (1) extended mode: $0.1 < P_{i,\mathrm{int}}/P_{i,\mathrm{tot}} < 0.28$, $0.1 < P_{i,\mathrm{AlN}}/P_{i,B} \leqslant 10$; (2) partially extended mode: $0.1 < P_{i,\mathrm{int}}/P_{i,\mathrm{tot}} < 0.28$, $P_{i,\mathrm{AlN}}/P_{i,B} \leqslant 0.1$ or $P_{i,\mathrm{AlN}}/P_{i,B} > 10$; (3) isolated mode: $P_{i,\mathrm{int}}/P_{i,\mathrm{tot}} < 0.1$; (4) localized mode: $P_{i,\mathrm{int}}/P_{i,\mathrm{tot}} > 0.28$. By calculating the lattice dynamics of the compositional-change $Al_xGa_{1-x}N$/AlN system ($x = 0$, 0.2, 0.5, 0.8), we first extracted the mode numbers of different interface phonon modes [Fig. 3(e)]. As the Al fraction x in $Al_xGa_{1-x}N$ increases, the mode ratios of four types of interface phonon modes are varied, where the number of states for localized modes is decreased and extended modes gradually dominate the interface phonon transition. The interface vibration amplitude of different modes follows a more concentrated distribution around the average amplitude [Fig. 3(f)] with increasing x, indicating the reduced amplitude of localized modes. These decreased number of states and vibration amplitude for localized modes may account for the diminished fitting residual of interface particular ingredient for the $Al_xGa_{1-x}N$/AlN system.

In order to clarify the influence of such interface phonon modes on the ITC, we performed molecular dynamics (MD) simulations using the interface conductance modal analysis (ICMA) formalism (Fig. 4).[46] The equilibrium MD simulations were performed using the LAMMPS package with the Stillinger–Weber (SW) potential.[47,48] The modal heat flux was calculated from modified LAMMPS.[49] In each simulation, initial structure was firstly relaxed under temperature control at 300 K

using velocity-rescaling. The heat flux was then calculated while running the simulation in the microcanonical ensemble for 350 ps with a time step of 1 fs. The modal contribution to ITC was then calculated as correlation of modes decomposed using the DFPT-calculated phonon eigenvectors as the basis vectors. The ITC of different ingredients decomposed into correlation integral maps between phonon modes sorted by their interfacial amplitude are shown in Figs. 4(a)–4(d). The eigenvectors are multiplied by a global scaling factor, such that the mean value of all modes' interfacial amplitude is equal to 1, labeled as the black dashed line in Figs. 4(a)–4(d). The greater value of normalized amplitude indicates the stronger vibration at the interface. The higher intensity in the region of localized modes (normalized amplitude > 1, right top region) illustrates that those interfacial vibrations actually enhance the contributions to the thermal conductivity, while the isolated modes (at left bottom of the map) show few contributions to the ITC. In addition, as the Al fraction increases, we observed the lower intensity of the right top region in correlation integral maps, indicating the decreased interaction between localized modes and other modes. Then we extract modal contributions to ITC associated with the four classes of interface phonon modes as shown in Figs. 4(e) and 4(f). Due to the large overlap of phonon DOS among $Al_xGa_{1-x}N$ based compounds, the extended mode mainly contributes to the total ITC. Moreover, the contribution of extended modes is monotonically higher while the influence of other three modes decreases as the Al fraction increases. Interestingly, the per-mode contribution of extended modes [Fig. 4(f)] is almost invariable with the compositional change. For localized modes, they own the highest contribution to ITC on per mode basis ($\sim 60.8\%$) at the GaN/AlN interface, similar to previous report on other interface systems.[34,43,50–52] As the Al fraction increases, their per-mode contribution to ITC decreases, consistent with the reduced intensity of correlation integral map with the Al fraction increases. By now, we have established the direct picture of the compositional fluctuation contributing to thermal transports across the interface. It can be seen that even a subtle concentration variation will highly affect the mode ratio and thermal conductivity contribution of different interface phonon modes, affecting the ITC.

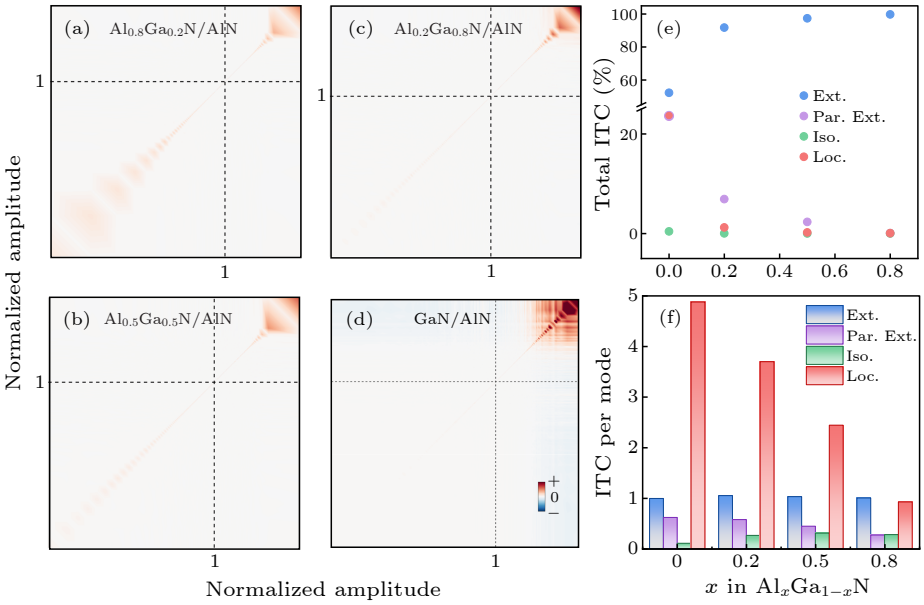

Fig. 4. Decomposition of interface thermal conductance into modal heat flux correlation integrals: (a)–(d) The magnitudes of the per-mode contribution to ITC sorted by their amplitude at the $Al_{0.8}Ga_{0.2}N$/AlN interface (a), $Al_{0.5}Ga_{0.5}N$/AlN interface (b), $Al_{0.2}Ga_{0.8}N$/AlN interface (c), and GaN/AlN interface (d), which is sensitive to the Al concentration. With the increased x value in $Al_xGa_{1-x}N$, it shows reduced intensity in the top right-hand corner of the mapping, signifying the increasingly weaker correlation between the localized modes and all the other modes. The axis illustrates the scale of interfacial amplitude. The dashed black curves represent the mean value of bulk vibration. A value greater than 1 means an enhanced vibration at the interface and a value smaller than 1 indicates a reduced vibration at the interface. The enhanced intensity in the top right-hand corner of the mapping signifies that large amplitude of vibrations at the interface greatly contributes to ITC, while modes with reduced amplitude at the interface show few contributions to ITC. (b) The changes of contribution to total ITC from four different classes of interface phonon modes with the Al fraction change in $Al_xGa_{1-x}N$. (c) The changes of the per-mode contribution to ITC from four different classes of interface phonon modes with the Al fraction change in $Al_xGa_{1-x}N$.

By systematically investigating the phonon-interface scattering in the compositional varied $Al_xGa_{1-x}N$/AlN system, we reveal the effects of local composition heterogeneity induced interfaces on the phonon transport and advance the understanding of the local thermal conductivity in practical nonuniform solids. With the Al fraction increasing, the smaller mismatch between the two adjoined bulks results in the reduced vibrational mode numbers and

amplitude of those localized modes at the interface, subsequently contributing smaller to ITC. In addition to the well-established knowledge of effects of mass disorder and strain fluctuations on local thermal properties, this work suggests that the compositional interface also plays an important role in the local thermal conductivity. The tunable interfacial thermal characteristics via compositional fluctuations tailoring interface phonon modes also provide new insights into the engineering of thermal properties in heat dissipation and energy conversion materials and devices.

Acknowledgments. The work was supported by the National Key R&D Program of China (Grant No. 2019YFA0708200), the National Natural Science Foundation of China (Grant Nos. 52125307, 11974023, 12104017, and 52021006), the "2011 Program" from the Peking-Tsinghua-IOP Collaborative Innovation Center of Quantum Matter, Youth Innovation Promotion Association, CAS. We acknowledge Electron Microscopy Laboratory of Peking University for the use of electron microscopes. We acknowledge High-performance Computing Platform of Peking University for providing computational resources for the DFPT calculation.

References

[1] Venkatasubramanian R, Siivola E, Colpitts T, and O'quinn B 2001 *Nature* **413** 597
[2] Rowe D M 2018 *Thermoelectrics Handbook: Macro to Nano* (Boca Raton: CRC Press)
[3] Waldrop M M 2016 *Nature* **530** 144
[4] Meneghesso G, Verzellesi G, Danesin F, Rampazzo F, Zanon F, Tazzoli A, Meneghini M, and Zanoni E 2008 *IEEE Trans. Device Mater. Relib.* **8** 332
[5] Ren J and Zhu J X 2013 *Phys. Rev. B* **87** 241412
[6] Li N B, Ren J, Wang L, Zhang G, Hänggi P, and Li B W 2012 *Rev. Mod. Phys.* **84** 1045
[7] Poudel B, Hao Q, Ma Y, Lan Y, Minnich A, Yu B, Yan X, Wang D, Muto A, Vashaee D, Chen X, Liu J, Dresselhaus M S, Chen G, and Ren Z 2008 *Science* **320** 634
[8] Qian X, Zhou J, and Chen G 2021 *Nat. Mater.* **20** 1188
[9] Tan G J, Zhao L D, and Kanatzidis M G 2016 *Chem. Rev.* **116** 12123
[10] Su L Z, Wang D Y, Wang S, Qin B, Wang Y, Qin Y, Jin Y, Chang C, and Zhao L D 2022 *Science* **375** 1385
[11] Vineis C J, Shakouri A, Majumdar A, and Kanatzidis M G 2010 *Adv. Mater.* **22** 3970
[12] Bu Z L, Zhang X Y, Shan B, Tang J, Liu H X, Chen Z W, Lin S, Li W, and Pei Y 2021 *Sci. Adv.* **7** eabf2738
[13] Abeles B 1963 *Phys. Rev. B* **131** 1906
[14] Dresselhaus M S, Chen G, Tang M Y, Yang R G, Lee H, Wang D Z, Ren Z F, Fleurial J P, and Gogna P 2007 *Adv. Mater.* **19** 1043
[15] Wu H J, Zhao L D, Zheng F S, Wu D, Pei Y L, Tong X, Kanatzidis M G, and He J Q 2014 *Nat. Commun.* **5** 4515
[16] Androulakis J, Lin C H, Kong H J, Uher C, Wu C I, Hogan T, Cook B A, Caillat T, Paraskevopoulos K M, and Kanatzidis M G 2007 *J. Am. Chem. Soc.* **129** 9780
[17] Lian H, Kumar A, Ocelík V, Baas J, Momand J, Kooi B J, and Blake G R 2021 *J. Mater. Chem. A* **9** 12340
[18] Lee S M, Cahill D G, and Venkatasubramanian R 1997 *Appl. Phys. Lett.* **70** 2957
[19] Garg J and Chen G 2013 *Phys. Rev. B* **87** 140302
[20] Swartz E T and Pohl R O 1989 *Rev. Mod. Phys.* **61** 605
[21] Zeiger P M and Rusz J 2021 *Phys. Rev. B* **104** 104301
[22] Gordiz K and Henry A 2016 *J. Appl. Phys.* **119** 015101
[23] Gordiz K and Henry A 2017 *J. Appl. Phys.* **121** 025102
[24] English T S, Duda J C, Smoyer J L, Jordan D A, Norris P M, and Zhigilei L V 2012 *Phys. Rev. B* **85** 035438
[25] Koh Y K, Cao Y, Cahill D G, and Jena D 2009 *Adv. Funct. Mater.* **19** 610
[26] Schelling P K, Phillpot S R, and Keblinski P 2002 *Appl. Phys. Lett.* **80** 2484
[27] Giri A and Hopkins P E 2020 *Adv. Funct. Mater.* **30** 1903857
[28] Krivanek O L, Lovejoy T C, Dellby N, Aoki T, Carpenter R W, Rez P, Soignard E, Zhu J, Batson P E, Lagos M J, Egerton R F, and Crozier P A 2014 *Nature* **514** 209
[29] Hage F S, Radtke G, Kepaptsoglou D M, Lazzeri M, and Ramasse Q M 2020 *Science* **367** 1124
[30] Senga R, Suenaga K, Barone P, Morishita S, Mauri F, and Pichler T 2019 *Nature* **573** 247
[31] Lagos M J, Trugler A, Hohenester U, and Batson P E 2017 *Nature* **543** 529
[32] Venkatraman K, Levin B D A, March K, Rez P, and Crozier P A 2019 *Nat. Phys.* **15** 1237
[33] Rez P, Aoki T, March K, Gur D, Krivanek O L, Dellby N, Lovejoy T C, Wolf S G, and Cohen H 2016 *Nat. Commun.* **7** 10945
[34] Qi R, Shi R, Li Y, Sun Y, Wu M, Li N, Du J, Liu K, Chen C, Chen J, Wang F, Yu D, Wang E G, and Gao P 2021 *Nature* **599** 399
[35] Yan X, Liu C, Gadre C A, Gu L, Aoki T, Lovejoy T C, Dellby N, Krivanek O L, Schlom D G, Wu R, and Pan X 2021 *Nature* **589** 65
[36] Simon J, Protasenko V, Lian C, Xing H, and Jena D 2010 *Science* **327** 60
[37] Chaudhuri R, Bader S J, Chen Z, Muller D A, Xing H G, and Jena D 2019 *Science* **365** 1454
[38] Gadre C A, Yan X, Song Q, Li J, Gu L, Huyan H, Aoki T, Lee S W, Chen G, Wu R, and Pan X 2022 *Nature* **606** 292
[39] Giannozzi P, Baroni S, Bonini N, Calandra M, Car R, Cavazzoni C, Ceresoli D, Chiarotti G L, Cococcioni M, Dabo I, Dal C A, De Gironcoli S, Fabris S, Fratesi G, Gebauer R, Gerstmann U, Gougoussis C, Kokalj A, Lazzeri M, Martin-Samos L, Marzari N, Mauri F, Mazzarello R, Paolini S, Pasquarello A, Paulatto L, Sbraccia C, Scandolo S, Sclauzero G, Seitsonen A P, Smogunov A, Umari P, and Wentzcovitch R M 2009 *J. Phys.: Condens. Matter* **21** 395502
[40] Ernzerhof M and Scuseria G E 1999 *J. Chem. Phys.* **110** 5029
[41] Vanderbilt D 1990 *Phys. Rev. B* **41** 7892
[42] Bungaro C, Rapcewicz K, and Bernholc J 2000 *Phys. Rev. B* **61** 6720
[43] Gordiz K and Henry A 2016 *Sci. Rep.* **6** 23139
[44] Qi R S, Li N, Du J, Shi R, Huang Y, Yang X, Liu L, Xu Z, Dai Q, Yu D, and Gao P 2021 *Nat. Commun.* **12** 1179
[45] Salje E K, Alexe M, Kustov S, Weber M C, Schiemer J, Nataf G F, and Kreisel J 2016 *Sci. Rep.* **6** 27193
[46] Gordiz K and Henry A 2015 *New J. Phys.* **17** 103002
[47] Stillinger F H and Weber T A 1985 *Phys. Rev. B* **31** 5262
[48] Zhou X W, Jones R E, Kimmer C J, Duda J C, and Hopkins P E 2013 *Phys. Rev. B* **87** 094303
[49] Seyf H R, Gordiz K, Deangelis F, and Henry A 2019 *J. Appl. Phys.* **125** 081101
[50] Cheng Z, Li R, Yan X, Jernigan G, Shi J, Liao M E, Hines N J, Gadre C A, Idrobo J C, Lee E, Hobart K D, Goorsky M S, Pan X, Luo T, and Graham S 2021 *Nat. Commun.* **12** 6901
[51] Li Y H, Qi R S, Shi R C, Hu J N, Liu Z T, Sun Y W, Li M Q, Li N, Song C L, Wang L, Hao Z B, Luo Y, Xue Q K, Ma X C, and Gao P 2022 *Proc. Natl. Acad. Sci. USA* **119** e2117027119
[52] Tian X Z, Yan X G, Varnavides G, Yuan Y K, Kim D S, Ciccarino C J, Polina A M Y L, Li L J, Narang P, Pan X, and Miao J 2021 *Sci. Adv.* **7** eabi6699